Interface resistance of $YBa_2Cu_3O_{7-\delta}/La_{0.67}Sr_{0.33}MnO_3$ ramp-type contacts

M. van Zalk,[1] A. Brinkman,[1] J. Aarts,[2] and H. Hilgenkamp[1,3]
[1]*Faculty of Science and Technology and MESA+ Institute for Nanotechnology, University of Twente, 7500 AE Enschede, The Netherlands*
[2]*Kamerlingh Onnes Laboratory, Leiden University, 2300 RA Leiden, The Netherlands*
[3]*Leiden Institute of Physics, Leiden University, 2300 RA Leiden, The Netherlands*
(Received 7 May 2010; revised manuscript received 5 September 2010; published 8 October 2010)

We fabricated and characterized $YBa_2Cu_3O_{7-\delta}/La_{0.67}Sr_{0.33}MnO_3$ (YBCO/LSMO) ramp-type contacts and junctions. An interlayer technique was applied to repair the ramp stoichiometry after etching. It was found that, typically, the resistance of the YBCO/LSMO interface is high compared to the resistances of YBCO interfaces to Au, Pt and the epitaxially grown ferromagnetic oxide $SrRuO_3$. The YBCO/LSMO interfaces were characterized electrically and were found to show a large negative, linear magnetoresistance. Electron energy loss spectroscopy experiments do not show a significant oxygen depletion near the YBCO/LSMO interface. Our results indicate that the high interfacial resistance is caused by the effect of charge transfer across the interface. The magnetoresistance suggests that part of the interface resistance is of magnetic origin.

DOI: 10.1103/PhysRevB.82.134513 PACS number(s): 74.78.Fk, 72.25.Mk, 73.40.Cg

I. INTRODUCTION

Studies on the $YBa_2Cu_3O_{7-\delta}/La_{0.67}Sr_{0.33}MnO_3$ (YBCO/LSMO) interface are of high importance because of the exotic properties of the constituents, namely, high-temperature superconductivity in YBCO and full spin polarization[1] in LSMO. The combination might give rise to several phenomena in the superconducting regime, such as spin-triplet supercurrents,[2–4] the superconducting spin-switch effect,[5–9] and crossed Andreev reflection.[10,11] In the normal-state regime, a transition from metallic to insulating behavior was reported for YBCO/$La_{0.67}Ca_{0.33}MnO_3$ (LCMO) superlattices,[12] related to a long range charge transfer between the two materials. A similar mechanism was mentioned to explain the observation of suppressed magnetization near this interface.[13] Recent experiments suggest orbital reconstructions and the formation of covalent Cu-Mn bonds over the YBCO/LCMO interface.[14] The influence of these effects on transport across cuprate/manganite interfaces remains elusive.

Many transport studies on YBCO/LSMO and YBCO/LCMO heterostructures focus on phenomena such as the suppression of T_c in such structures.[15,16] There is a number of studies that report on the transport properties of YBCO/LSMO junctions. Sawa *et al.*[17] investigated cross-strip junctions, in which they found a zero-bias conductance peak (ZBCP), pointing at the presence of an insulating ferromagnetic barrier. The role of Andreev bound states in planar junctions was discussed by Chen *et al.*[18] Mikheenko *et al.*[19] observed a resistance increase for decreasing temperatures in YBCO/LCMO planar junctions, which they suggested to stem from the interplay between spin polarization in LCMO and antiferromagnetic spin fluctuations in YBCO in the pseudogap state.

In this paper we will employ ramp-type contacts, prepared by positioning a top electrode over a ramp that was etched previously into the base electrode. In this configuration, transport takes place in the direction of YBCO's crystallographic *ab* plane, in which the superconducting coherence length is the largest. Furthermore, the fabrication process yields well-defined small-area junctions, allowing for a precise determination of the specific junction resistance, R_nA, and critical current density, J_c. Huang *et al.*[20] and Schoop *et al.*[21] report on the fabrication and characterization of YBCO ramp junctions with manganite barriers. Both measure large normal state resistances, largely exceeding the value expected from the bulk resistivity of the barrier material. Some of their junctions show supercurrents.

In our work we apply an interlayer technique (consisting of an *in situ* etch cleaning step of a predefined ramp in a YBCO base electrode, followed by the deposition of a YBCO interlayer, which restores the stoichiometry at the ramp, before the deposition of the top electrode), which was found to decrease the normal state resistance of high-T_c/low-T_c superconducting contacts by a factor of 10^4 (Ref. 22). It is expected that the interlayer technique can be useful for all-oxide junctions as well.

Despite the use of an interlayer, we find that the YBCO/LSMO interface is characterized by an unusually large contact resistance, which is the central theme of this research. We have compared different structures and replaced the LSMO by several other materials, in order to investigate the origin of the high resistance. A summary of the different structures used, can be found in Table I.

II. EXPERIMENTAL DETAILS

A. Sample fabrication

All structures were grown with pulsed laser deposition on $SrTiO_3$ (STO) substrates, which were chemically treated[23] and annealed for at least two hours at 950 °C in an oxygen flow to produce atomically flat, TiO_2-terminated surfaces. Deposition settings for the various materials are summarized in Table II. All junctions and contacts (see Fig. 1) were formed from a bilayer consisting of a 200 nm YBCO base electrode and a 100 nm STO insulation layer. After growth, the bilayer was cooled down to 600 °C and the oxygen pres-

TABLE I. Layer thicknesses (d) and materials for the different structures used in this research.

	Base YBCO	Interlayer YBCO	Barrier LSMO	Top electrode	
	d (nm)	d (nm)	d (nm)	d (nm)	Material
SFS1	200	7	8	100	YBCO
SFS2	200	7	30	100	YBCO
SF1	200	7		100	LSMO
SF2	200	20		100	LSMO
SF3	200	7		280	SRO
SN1	200	10		100	Au
SN2	200	7		100	Pt

sure was raised to slightly below atmospheric pressure. The sample was then cooled down to room temperature at a rate of 4 °C min^{-1}. The base electrode was defined by photolithography and a subsequent argon ion milling step under an angle of 45°, rotating in plane. This procedure typically yields a ramp angle of 20–30°. After removal of photoresist, the sample was placed back in the deposition chamber for the interlayer and top-electrode deposition. The exposed ramp was first cleaned by (perpendicular) argon ion milling in two steps: a 500 V etch to remove amorphous material from the ramp, and a 50 V step to improve the smoothness of the ramp. A thin YBCO interlayer was grown using standard YBCO deposition settings, followed by a barrier (if present) and top electrode. Cooldown was performed according to the procedure described above. For Au and Pt top electrodes, the sample was annealed first and cooled down to 100 °C, before deposition of the top electrode. Definition of the top electrode was done by photolithography and argon ion milling. The overetch was kept small to prevent the STO surface from becoming conductive. In a few cases, a 600 °C reanneal in oxygen was necessary to restore insulating behavior. On each sample were 9 junctions with widths of 10 and 40 μm. Lastly, Ti/Au contact pads were fabricated by sputter deposition and lift-off.

B. Electrode characterization

The design of the top electrode [see Fig. 1(a)] allowed its separate electrical characterization. The YBCO top electrode showed a T_c varying from 78 to 89 K. For LSMO, resistance-versus-temperature [$R(T)$] measurements had the typical LSMO bell shape, with the maximum at 310 K. The SRO top electrodes showed a Curie temperature of 140 K, as determined from a kink in the $R(T)$ curve.

TABLE II. Pulsed laser deposition settings for the materials used in this research.

Material	Laser fluence (J cm^{-2})	Temperature (°C)	Pressure (mbar)
YBCO	1.5	780	0.25 O_2
LSMO	2.0	800	0.16 O_2
SRO	2.5	600	0.13 O_2
STO	1.5	740	0.10 O_2
Au	3.5	100	0.22 Ar
Pt	4.3	100	0.10 Ar

It was found that in these all-oxide epitaxial structures the interlayer can become superconducting at much smaller thicknesses than when covered by a Au or Pt top electrode. In the latter case we did not observe superconductivity in 10 nm thick interlayers. When underneath LSMO or SRO, even 7 nm interlayers turn superconducting with a maximum T_c of 25 K. However, a superconducting current path shunting the junction was only observed for SF2, which has a 20 nm interlayer. The absence of a continuous superconducting current path through 7 nm YBCO interlayers implies that the interlayer is nonsuperconducting at the bottom of the ramp, i.e., at part B as indicated in Fig. 1(b). This point will be further discussed in Sec. III B.

Electrode contributions from nonsuperconducting electrodes were subtracted to find the intrinsic contact resistance. For that purpose, the top-electrode resistivity was measured locally near the contact.

C. Scanning SQUID microscopy

SFS1 has been examined in a scanning superconducting quantum interference device (SQUID) microscope.[24] The

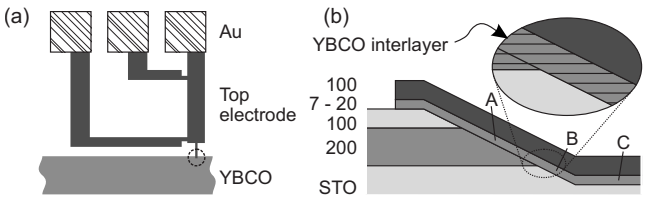

FIG. 1. (a) Geometry of the structures used in this paper. The contact/junction is indicated by a dashed circle. The local resistivity of the top electrode can be measured, in order to subtract the electrode contribution from the junction resistance, in the case of a nonsuperconducting top electrode. Junctions are 10 or 40 μm wide. (b) Schematic view of the junction cross section, with layer thicknesses as indicated (in nanometer), from bottom to top YBCO, STO, YBCO, and top electrode. Three distinct interlayer parts (A, B, C) can be identified. The magnified section shows the direction of the YBCO *ab* planes.

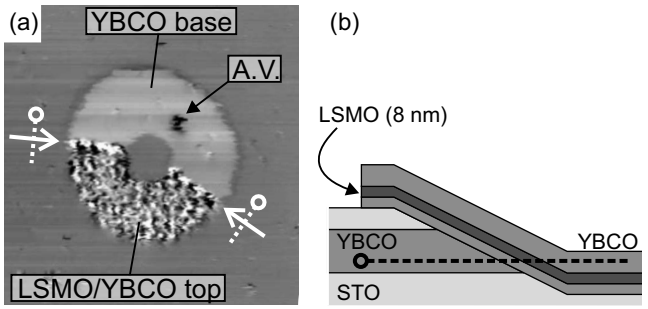

FIG. 2. (a) Scanning SQUID microscopy graph (4.2 K) of a ring-shaped structure (120 μm in diameter) comprising two 40 μm wide junctions (indicated by white arrows). The junction cross section is shown in (b). Despite the small thickness (8 nm) of the LSMO layer, the signal from the ferromagnetic domains is clearly detected at 4.2 K. The sample was cooled down in zero background magnetic field. An Abrikosov vortex (A.V.) is present in the base electrode.

sample contained a ring-shaped structure allowing a closed current path through the YBCO of the base and top electrode via two YBCO/LSMO/YBCO junctions. The sample was cooled down to 4.2 K in zero magnetic field. A pick-up loop with an effective area of about 10 μm^2 coupled to a SQUID magnetometer was scanned over the sample while in contact with the surface. In this way, the perpendicular component of the magnetic field at the sample surface is predominantly measured. The result is shown in Fig. 2(a). The YBCO base electrode is visible because its inductance is different from the substrate. Despite the small thickness of the LSMO layer of 8 nm, a magnetic signal is clearly visible. Stray fields from ferromagnetic domain walls penetrate the 100 nm thick superconducting layer covering the LSMO. The largest stray fields are observed near the junctions, due to the upward bending of magnetic field lines by the superconducting YBCO ramp, which is present underneath the LSMO barrier at this position.

D. Superconducting properties of YBCO/LSMO/YBCO junctions

The main theme of this paper is the interface resistance of our junctions. For completeness, we will briefly summarize here also their superconducting properties. On SFS1, roughly 50% of the junctions showed a supercurrent, the critical current densities J_c being in the range of 0.2–0.6 kA cm^{-2} and featuring I_cR_n (I_c is the critical current of the junction and R_n the normal state resistance) products of up to 2.5 mV at 4.2 K. (Throughout this paper, we use the full ramp area $A = Wd/\sin\alpha$, with W the junction width, d the thickness of the YBCO base electrode and α the ramp angle, for the determination of J_c and R_nA.) For comparison, J_c is typically 10–100 times larger in YBCO/Au/Nb interlayer ramp-type junctions.[22] When using an effective barrier thickness d_{eff} of 300 nm (the London penetration depth for YBCO is about 150 nm), we find a Josephson penetration depth $\lambda_J = \sqrt{\Phi_0/2\pi\mu_0 J_c d_{eff}} \approx 15$ μm (Φ_0 is the flux quantum, μ_0 the vacuum permeability). Upon microwave irradiation, Shapiro steps were observed clearly, however, the modulation of the critical current in a magnetic field applied parallel to the sample surface remained below 1% up to 1 mT. For the given λ_J, a larger modulation could be expected for a homogeneous Josephson junction. In SFS2, only one junction showed a supercurrent, and the modulation in magnetic field showed a typical SQUID-like periodic pattern. This is most likely caused by the presence of separate pinholes in this specific junction. The high I_cR_n values and absence of field dependence in the other junctions that show supercurrents, strongly point in the direction of the presence of pinholes in these junctions too. We did not find unambiguous Josephson junction behavior in one of our samples. The presence of pinholes did not strongly influence the junction R_nA. All junctions exhibit R_n values within the same range and the influence of pinholes on R_n is therefore negligible, pointing at small pinhole sizes. We have not excluded the junctions with pinholes from the analysis of the interface resistance.

III. EXPERIMENTAL RESULTS

A. YBCO/LSMO/YBCO junctions

The normal state resistances of junctions on samples SFS1 and SFS2 at 4.2 K are displayed in Fig. 3(a). Although the data show a large spread around the mean, the normal state resistances are on average unusually high. For the YBCO/LSMO/YBCO junctions, we find a logarithmic average of 2.6 $\mu\Omega$ cm^2 (the normal average yields 3.5 $\mu\Omega$ cm^2). This number exceeds the resistance that can be expected from the bulk LSMO resistivity by a factor of 10^3. For comparison, our YBCO/Au ramp-type contact (SN1) showed an R_nA of 0.03 $\mu\Omega$ cm^2, which is equal to the value reported for YBCO/Au/Nb ramp-type junctions.[22] The fact that SFS2 tends to have a somewhat lower interface resistance than SFS1, despite the LSMO barrier being thicker, is likely due to the slightly smaller substrate-target distance that was used for SFS2, which resulted in a higher quality of epitaxial growth, as witnessed by a smaller peak width in x-ray diffraction measurements.

We characterized one of the junctions (with no measurable supercurrent) on SFS1, by recording a differential conductance spectrum, $dJ/dV(V)$, measuring the temperature dependence of its resistance and the magnetoresistance [Figs. 3(b)–3(d)]. The conductance spectrum measured at 2 K clearly shows a ZBCP. The width of this peak is larger than the conductance peaks due to supercurrents usually are and therefore cannot be attributed to the presence of a small supercurrent in the junction. The conductance spectrum further shows a linear background conductance and a kink at 18 mV. In all these details the spectrum compares well to data obtained from YBCO/LSMO cross-strip junctions that are reported in the literature.[17] The presence of a ZBCP implies either an incomplete spin polarization of the LSMO (Ref. 25) or the presence of domain walls. In Fig. 2, we have seen that domain walls can be present in our junctions. The formation of bound states is, however, still surprising since in our geometry the angle between the interface normal and YBCO antinodal direction is close to zero. ZBCP's in that case might be an indication for faceting of the YBCO ramp, or

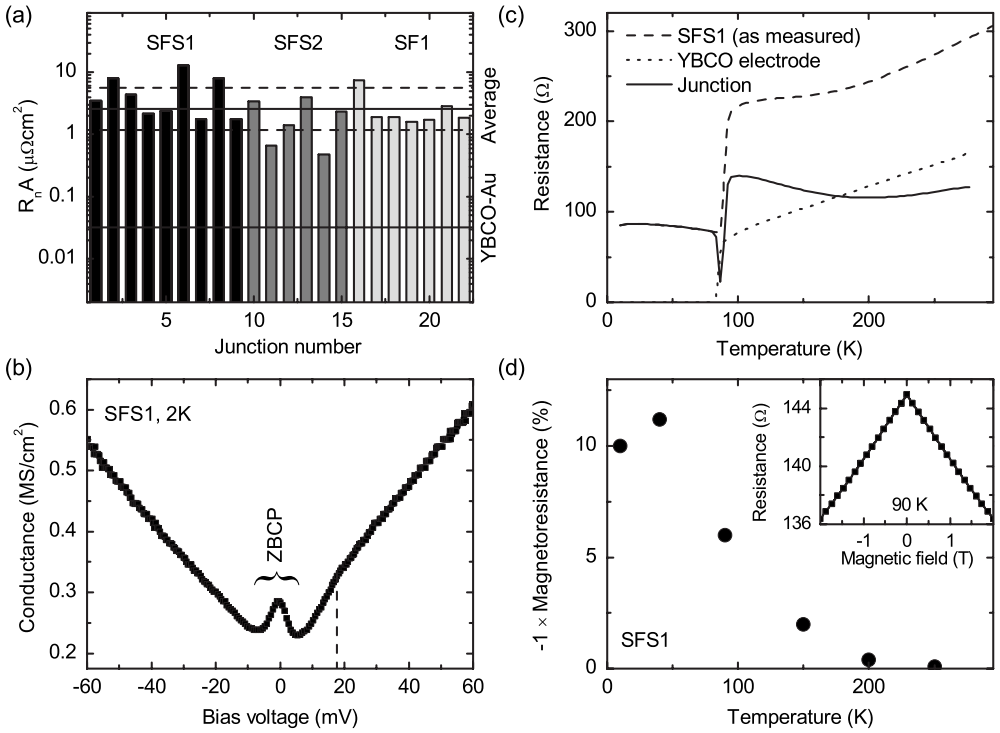

FIG. 3. (a) Summary of the specific resistances at 4.2 K of 15 YBCO/LSMO/YBCO junctions and 7 YBCO/LSMO contacts on three different samples. The logarithmic average yields 2.6 $\mu\Omega$ cm^2. The logarithmic standard deviation is indicated by dashed lines. For comparison, the resistance of YBCO/Au junctions is indicated in the graph as well. (b) The conductance spectrum of one of the 10 μm wide SFS1 junctions at 2 K. It features a ZBCP, a linear background and a kink at 18 mV (indicated by a dashed line). (c) Temperature dependence of the junction resistance. The dashed line is as measured and the solid line is with the electrode contribution (dotted line) subtracted. The T_c's of the top and base electrode cannot be distinguished. Below T_c, the junction resistance shows a maximum at 25 K and above T_c, a minimum near 200 K. (d) The junction resistance exhibits a linear, negative magnetic field dependence (shown in the inset). The magnetoresistance (at 2 T) is shown for different temperatures. The magnetoresistance vanishes above 200 K.

have a completely different explanation, such as the Anderson-Appelbaum model.[26]

Figure 3(c) depicts the temperature dependence of the junction resistance. The result is representative for other junctions on SFS1 and SFS2. The transition temperatures of the base and top electrode (89 K) cannot be distinguished. Above T_c, we have subtracted the YBCO electrode contribution yielding the bare junction resistance. It shows a minimum around 200 K. Below T_c the junction resistance increases and shows a maximum at 25 K. The decrease in resistance below that temperature is caused by the developing ZBCP at low temperature. The sharp dip around T_c of the YBCO electrode is an artifact of the subtraction procedure. The junction resistance is discontinuous around T_c. We believe that the discontinuity is real since if the electrode contribution would be larger than expected, the discontinuity can be lifted but the junction resistance would turn negative around $T=200$ K. The discontinuity could be caused by superconductivity penetrating for some distance into the barrier. As discussed in Sec. II D, some junctions on SFS1 contain pinholes. Although we do not know the exact nature of the pinholes, whether it is a physical hole in the barrier or a percolation path of defects, we can imagine that it extends into the barrier for some distance without penetrating it. This way, the effective barrier thickness might be affected by the YBCO turning superconducting.

Ramp-type junctions fabricated without interlayer sometimes show a strongly increasing resistance for low temperatures.[20,21] This is apparently diminished by the use of an interlayer. Our junction resistances compare well to the literature values for selected junctions that do not show such a strong increase.[17,21]

Figure 3(d) shows the magnetoresistance, $[R(2\ \mathrm{T}) - R(0\ \mathrm{T})]/R(0\ \mathrm{T})$, of the junction as a function of temperature. The negative and linear magnetoresistance vanishes above 200–250 K, which coincides with the minimum in the $R(T)$ measurement. This point will be discussed in more detail in Sec. IV.

B. YBCO/LSMO contacts

In addition to junctions, we have also fabricated YBCO/LSMO contacts and determined the interface resistance at 4.2 K by subtraction of the electrode contribution. The values found are comparable to the ones found for the junctions, indicating that the resistance stems from the YBCO/LSMO interface. A possible factor of 1/2 due to the fact that the contacts contain a single YBCO/LSMO interface and the junctions two, cannot be resolved due to the scatter of the data.

As was noted in Sec. II A, the interlayer of SF1 underneath the LSMO top electrode [region C in Fig. 1(b)] be-

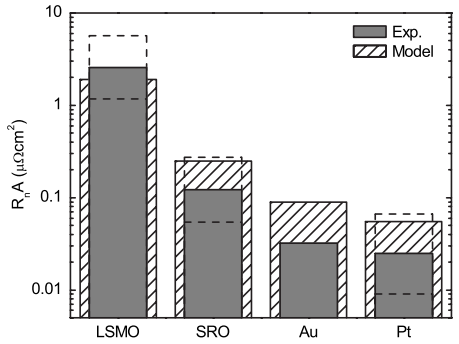

FIG. 4. Summary of the interface resistances (narrow, gray bars) for contacts with YBCO for different materials. Logarithmic standard deviations are indicated by dashed lines. All resistances are determined at 4.2 K. The wider, hatched bars are estimates from a Schottky junction model as described in Sec. IV.

comes superconducting below 25 K despite its small thickness of 7 nm. However, the contact resistance does not vanish when the interlayer becomes superconducting, indicating the absence of a superconducting path between the interlayer part C and the YBCO base electrode. Most likely, the nonsuperconducting region is part B of the interlayer, grown on the bottom of the ramp. The current is then forced to pass through the LSMO electrode and the YBCO/LSMO interface. It is an interesting possibility that the suppression of superconductivity in part B of the interlayer is induced by the proximity of the LSMO, similar to the suppression observed for *c*-axis YBCO/LCMO superlattices.[12,16,27] The fact that superconductivity is not suppressed in part C of the interlayer could be explained by a less effective coupling in the *c*-axis direction. We have increased the interlayer thickness to 20 nm for SF2 and for this case we did observe a superconducting path over the ramp. We thus know that a possible suppression of superconductivity in YBCO by contact with LSMO in the *ab* direction takes place over length scales smaller than 20 nm.

C. Comparison to other materials

Variation in top-electrode material can shed light on the origin of the unusually large normal-state resistance of the YBCO/LSMO contacts. One sample was prepared using the oxide ferromagnet $SrRuO_3$. Although in the bulk, SRO is orthorhombic, it is very close to the cubic perovskite structure.[28] It can grow fully coherently on STO. Our x-ray measurements show a slightly elongated lattice constant in the *c* direction of 3.95 Å whereas the pseudocubic lattice constant is 3.93 Å; most likely, the elongation is caused by the epitaxial compressive strain from the STO substrate. The difference in lattice constant of less than 2% compared to LSMO, together with the fact that both materials are grown at high temperatures and exposed to the same annealing procedure, justify a direct comparison of the two materials. We also fabricated YBCO/Au and YBCO/Pt contacts. The gray bars in Fig. 4 summarize the results (the wider, hatched bars are calculated results of the Schottky junction model as will be discussed in Sec. IV). The number of contacts measured to determine the average R_nA were 4 and 5 for SRO and Pt, respectively.

The contact resistances of YBCO/Au and YBCO/Pt are on average more than 50 times lower than for YBCO/LSMO. The transparencies of these contacts are themselves already quite low. We estimated a Sharvin resistance for YBCO/Au to be about 10^{-10} Ω cm^2, even when taking into account the mismatch in Fermi velocities of YBCO and Au.

The average R_nA of 0.1 $\mu\Omega$ cm^2 for the YBCO/SRO contacts is lower by more than a factor of 20 than for the YBCO/LSMO interfaces. This indicates that the high resistance of the latter cannot be an effect of ferromagnetism alone, although it might contribute. The YBCO/SRO values compare reasonably well to values listed in the literature[29,30] but the average value and the spread might be slightly smaller in our case due to the application of the interlayer.

IV. ORIGIN OF THE INTERFACE RESISTANCE

There are several possible explanations for the large resistance of the YBCO/LSMO interface. These can be divided into (1) electronic effects, such as charge transfer, (2) spin effects due to the spin-polarized nature of LSMO, and (3) structural effects, such as defects and oxygen vacancies.

Many studies have demonstrated the possibility of epitaxial growth on YBCO etched ramps.[22,31–33] In transmission electron microscope images, the boundary between the YBCO ramp and the interlayer is indiscernible.[22] Nevertheless, the possibility remains that the material grown on the ramp possesses an increased number of defects, which can lead to bad conductivity. The mere presence of elastic scatter centers cannot account for the high R_nA value for YBCO/LSMO interfaces. Assuming that the interface resistance comes from a region less than 10 nm thick, which is likely from the discussion in Sec. III B, the specific resistivity, ρ, would have to be larger than 2 Ω cm for LSMO. Within the Drude model, we estimate the scattering time τ from $\rho = m_e/ne^2\tau$, with m_e, n, and e the electron mass, density and charge, respectively. From $l_e = v_F\tau$, with v_F the Fermi velocity, we conservatively estimate the mean free path $l_e < 0.02$ Å, much smaller than the interatomic distance. The resistance arising from elastic scattering is thus unlikely.

Instead, the presence of a carrier depleted insulating or nearly insulating region more likely underlies the high R_nA. An often suggested cause for insulating behavior is oxygen off-stoichiometry at the interface. There are two possible reasons for such an off-stoichiometry to arise: (1) the migration of oxygen from one material to the other and (2) the creation of vacancies or interstitial oxygen near the interface as a result of epitaxial strain.

Possibility (1) can be expected if it is accompanied by a lowering of the Gibbs free energy. We estimate whether this is the case by comparing the free energy changes upon oxidation[34] for the individual elements in the materials under study. For Au and Pt, the free energy change is positive and it is therefore unlikely that these materials would take up oxygen out of the YBCO. The largest free energy decrease (per oxygen atom and at 300 K) is shown by Y, followed by La, Sr, Ba, Mn, Cu, and Ru, the latter two significantly

smaller than the others. Therefore, oxygen migration is expected to be the strongest from YBCO to LSMO and to a lesser degree from YBCO to SRO, or perhaps even from SRO to YBCO. The increasing tendency for oxygen migration in YBCO/Pt, YBCO/Au, YBCO/SRO, and YBCO/LSMO junctions is thus compatible with the observed increasing junction R_nA for these interfaces. We note, however, that in the process of epitaxial growth and in the subsequent annealing step, abundant oxygen is present. Under such circumstances, single thin films are fully oxidized and it can be questioned why this would not be the case for heterostructures consisting of two materials.

The interplay between oxygenation and strain [scenario (2)] was clearly demonstrated in the cuprate parent compound La_2CuO_4.[35] In the present case the lattice mismatch between LSMO (a=3.885 Å) and YBCO in the direction of the chains (b=3.88 Å) is nearly zero. LSMO thus does not hinder the uptake of oxygens in the YBCO chains and an oxygen deficiency due to strain seems unlikely. SRO has a slightly larger lattice constant (3.95 Å in the c direction and likely some 3.92 Å in the a and b directions, assuming the volume of the unit cell remains constant under strain). As a result, oxygen at interstitial sites might be present. The additional oxygen would donate holes to the YBCO CuO_2 planes. The interfacial resistance of YBCO/SRO is indeed smaller than that of YBCO/LSMO. Although both oxygen off-stoichiometry scenarios (1) and (2) are consistent with the observed trends, there are some unsatisfactory features.

We estimate from literature values for the resistivity of strongly oxygen depleted YBCO (with on average 6.2 oxygen atoms per unit cell) (Ref. 36) that a 10–100 nm oxygen deficient layer would be needed to explain the YBCO/LSMO interface R_nA. The presence of such a layer would be reflected in a strongly increasing resistance with decreasing temperatures, which is incompatible with our experimental results. Because of the inert nature of Au and Pt, oxygen off-stoichiometry is unlikely for the YBCO/Pt and YBCO/Au contacts. Nevertheless, these contacts exhibit a low transparency as was mentioned before, suggesting that oxygen depletion cannot be in general the only reason for large YBCO contact resistances. This latter argument of course cannot exclude a possible contribution of oxygen depletion to the YBCO/LSMO and YBCO/SRO interfaces.

As a test for the presence of oxygen off-stoichiometry near the YBCO/LSMO interface, we have performed electron energy loss spectroscopy (EELS) on the ramp region of SF1. With a focused ion beam, a transmission electron microscopy (TEM) specimen was prepared, allowing a cross-sectional view of the YBCO/LSMO contact. Using energy-filtered TEM, images were recorded before and after the ionization edge of the O K shell.[37] An oxygen mapping was obtained by subtracting the pre-edge image from the post-edge image. The result is shown in Fig. 5. With the resolution we could achieve and a detection limit of about 5%,[37] it seems clear that the oxygen content of the YBCO and LSMO film is homogeneous to within at least 10 nm of the ramp and we find no indications for a 10–100 nm oxygen deficient layer. We therefore conclude that, although we cannot fully exclude the influence of oxygen off-stoichiometry, an additional mechanism leading to interface resistivity must be active.

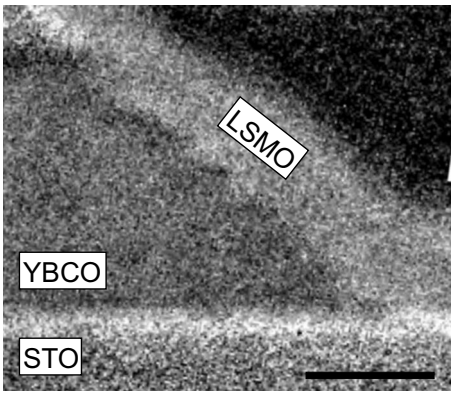

FIG. 5. Oxygen mapping of the junction obtained with EELS. Oxygen depletion near the YBCO/LSMO interface is below the detection limit. Note the increased intensity at the YBCO/STO interface. The scale bar denotes 100 nm.

A candidate is the electronic mechanism of charge transfer across the interface, which was proposed to be of importance to interfaces involving cuprate superconductors.[38,39] The transfer of charge can lead to the formation of a charge carrier depleted region on one or both sides of the junction, which gives rise to interface resistance. For YBCO/metal interfaces, the formation of a Schottky barrier can be expected as for semiconductor/metal interfaces. Schottky barriers result from work function differences between the semiconductor and the metal. A Schottky barrier was suggested to cause the low interface transparency of YBCO/Au and YBCO/Pt interfaces.[22] Tunnel experiments with YBCO/Au/Nb junctions have indeed demonstrated the presence of a tunnel barrier at the YBCO/Au interface.[40]

The transfer of charge across the YBCO/LCMO interface was suggested by several experiments.[12,13] Theory predicts a 2–3 unit cell thick antiferromagnetic insulating region in the cuprate resulting from charge transfer, which also for this interface is driven by the work function difference between YBCO and LCMO.[41] However, the phase diagrams of strongly correlated materials are complex and rich and substantial deviations from ideal Schottky behavior can be expected. Schottky behavior would be easily recognizable in current-voltage-characteristics from the rectifying properties of the Schottky junction. We have indeed measured some asymmetry in the YBCO/LSMO conductance for opposite polarities [Fig. 3(b)]. For the low-bias voltages at which we have measured, no strong rectification can be expected. Moreover, the conductance spectrum for the YBCO/LSMO junction is dominated by a linear background which might have an origin unrelated to the Schottky junction.[42]

It is instructive to obtain an estimate of the interface resistances for the various material combinations from the Schottky junction model. The picture we have in mind is sketched in Fig. 6. YBCO is depicted as a p-type degenerate semiconductor, with the Fermi energy below the band gap in the valence band. As a result of the work function difference between YBCO and LSMO, the YBCO bands bend downward. This leads to the depletion of holes in the YBCO near the interface. Transport through the junction is expected to be dominated by tunneling (instead of thermionic emission)

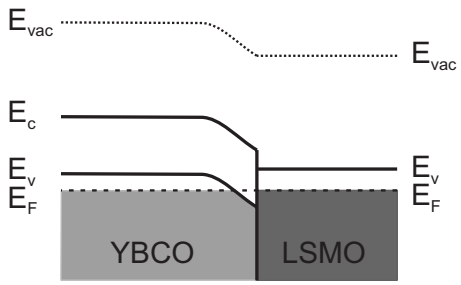

FIG. 6. Schematic view of the band-bending picture for the YBCO/LSMO interface. The larger work function of YBCO leads to a downward bending of the bands and consequently to a depletion of holes near the interface.

because the high-carrier density leads to a small depletion width. The appropriate regime is determined by E_{00}, defined by $E_{00} \equiv e\hbar\sqrt{n/m_e\epsilon_r\epsilon_0}/2$ with $\hbar$ the reduced Planck constant, ϵ_r and ϵ_0 the relative and vacuum permittivity, respectively. The condition $E_{00} \gg k_B T$ (k_B being the Boltzmann constant) is fulfilled, which means that the junction is in the tunneling regime.[43] The junction resistance then follows from[43]

$$R_n A = \frac{k_B \sin \pi c_1 k_B T}{A^{**} \pi e T} \exp \frac{\phi}{E_{00}}, \tag{1}$$

with

$$c_1 = \frac{1}{2E_{00}} \ln \frac{4\phi}{E_v - E_F}. \tag{2}$$

Here ϕ is the Schottky barrier height, which for the ideal Schottky junction is equal to the difference between the work functions of the two materials. For the effective Richardson constant A^{**} we take the free electron value of 120 $A/cm^2\,K^2$ and we further use the parameters $n \approx 10^{21}$ cm^{-3}, $\epsilon_r \approx 30$ (Ref. 44) and for the energy separation between the Fermi energy and the valence band $E_v - E_F \approx 0.1$ eV (Ref. 45).

The work function of LSMO is 4.8–4.9 eV.[46–48] Au and Pt have work functions of 5.1 eV and 5.65 eV, respectively.[49] For SRO, the values in the literature vary from 5.0–5.2 eV.[48,50–52] The interface resistance of the YBCO/SRO interface is larger than that of the YBCO/Au interface, which implies a larger energy barrier. We therefore take the value of 5.0 eV for SRO. The scatter in work-function data for YBCO is particularly large, 5–6 eV: a work function of about 5 eV was found in Refs. 53–55 whereas values up to 6 eV and even higher were reported in Refs. 56 and 57. If we take the YBCO work function to be 5.6 eV, we evaluate the junction $R_n A$ for LSMO, SRO and Au as indicated by the shaded bars in Fig. 4 For Pt, the work function is almost equal to 5.6 eV, which would yield a vanishingly small $R_n A$. However, the effective work function of Pt, when grown on HfO_2, is reduced to 5.15 eV.[58] We used this value for the YBCO/Pt $R_n A$ estimate in Fig. 4. We like to stress here that the calculation of the Schottky resistance only serves as an illustration and is not meant to argue that the interfaces described in this paper behave as ideal Schottky junctions. Nevertheless, the estimated values are quite well in the range of the experimental

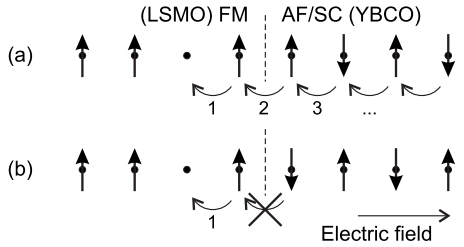

FIG. 7. Schematic view of a possible mechanism leading to interfacial resistance due to the combination of a high degree of spin polarization in the ferromagnet and antiferromagnetic spin fluctuations in the superconductor. A similar mechanism was suggested in Ref. 19. In (a) the hole in the ferromagnet can freely penetrate into the superconductor under the applied electric field as indicated in the picture. However, in the situation depicted in (b), the hole will be blocked at the interface since the spin-down electron cannot hop into the ferromagnet.

ones. We have not taken into account deviations from ideal Schottky behavior, such as the presence of surface states, which lead to a work function independence of the Schottky barrier.[43] This might be an alternative explanation of why the YBCO/Pt resistance is comparable to the YBCO/Au resistance.

The width of the charge carrier depleted region can within the Schottky model be estimated from the values we have found for the barrier height by using the standard expression $x_d = \sqrt{2\epsilon_r\epsilon_0\phi/e^2 n}$. We find values in the range of 3–4 unit cells, which corresponds roughly to the 2–3 unit cells found by Yunoki *et al.*[41] by static and dynamical mean-field theory. It is well known that the undoped cuprate parent compounds are antiferromagnetic insulators and antiferromagnetism is also expected for the depletion region near YBCO interfaces.[41] One might wonder what consequences the antiferromagnetic surface layer would have for transport into the highly spin polarized LSMO. Figure 7 presents a sketch of the situation arising at the YBCO/LSMO interface. There are two distinct situations. In (a), a hole coming from the side of the LSMO can freely cross the interface, which results in a new configuration of spins in the YBCO as indicated in (b). A second hole will now be blocked at the interface since the spin-down electron in the YBCO is not allowed to hop into the LSMO. This simple picture suggests that in contacts between antiferromagnetically and ferromagnetically correlated materials a contribution to the interface resistance is present due to spin blocking effects. More thorough theoretical investigations are needed to corroborate this idea. Because of the two-dimensional nature of the interface and a finite antiferromagnetic correlation length, the interface resistance will not be infinite, as the schematic picture in Fig. 7 might suggest. Note that for the proposed mechanism the presence of a depletion layer is not strictly necessary. Even in the optimally doped cuprates antiferromagnetic correlations are present.[59–63]

Interface resistance of magnetic origin, such as caused by a mechanism as described above, is expected to respond to the application of magnetic field, due to domain reorientation effects in the ferromagnet. The situation is similar to the magnetoresistance observed in polycrystalline LSMO thin

films, which show magnetoresistance due to spin-polarized intergrain tunneling.[64] Interestingly, magnetoresistance appears in our junctions below 200 K, at which temperature also the interface resistance shows a minimum; see Fig. 3(c). Mikheenko *et al.*[19] have also reported increasing junction resistance for planar YBCO/LCMO contacts below 200 K, and associated this temperature with the pseudogap temperature. They argue that the increase in junction resistance below this characteristic temperature results from an interaction between the spin-polarized current and the antiferromagnetic spin fluctuations of the pseudogap state, an idea which is quite similar to the one described above.

V. CONCLUSION

We have observed an unusually large interfacial resistance for YBCO/LSMO interfaces, when compared to interfaces between YBCO and several other materials. We have shown that this is likely caused by the phenomenon of charge transfer and resulting carrier depletion in these interfaces, that has received a lot of attention in recent years.[12,13,41] In addition, a contribution related to the spin-polarized nature of LSMO might also be present.

The fundamental origin of the resistivity of YBCO interfaces has important consequences for the fabrication of devices. High-quality interfaces might face a lower boundary of the contact resistance, depending on parameters such as the work function of the material being contacted. In a planar geometry, accurate values for the YBCO/LSMO interface R_nA are difficult to obtain but they are not expected to be much smaller than the values we have obtained for *ab* contacts. For YBCO/noble metal interfaces, the resistance for a *c*-axis contact is even larger than for an *ab*-axis contact. For *c*-axis YBCO/LSMO and YBCO/LCMO heterostructures, it is often concluded from the atomical sharpness of the interfaces, that the contacts are electrically highly transparent. We challenge this assumption since the occurrence of charge transfer seems not to be restricted to unsharp interfaces.

ACKNOWLEDGMENTS

We acknowledge Patrick Grunder and Rico Keim for the TEM preparation and analysis. This work is part of the research program of the Foundation for Fundamental Research on Matter (FOM), financially supported by the Netherlands Organization for Scientific Research (NWO), and the NanoNed program. H.H. in addition acknowledges the NWO VICI grant.

[1] J. H. Park, E. Vescovo, H. J. Kim, C. Kwon, R. Ramesh, and T. Venkatesan, Nature (London) **392**, 794 (1998).
[2] R. S. Keizer, S. T. B. Goennenwein, T. M. Klapwijk, G. Miao, G. Xiao, and A. Gupta, Nature (London) **439**, 825 (2006).
[3] Y. Asano, Y. Tanaka, and A. A. Golubov, Phys. Rev. Lett. **98**, 107002 (2007).
[4] M. Eschrig and T. Löfwander, Nat. Phys. **4**, 138 (2008).
[5] L. R. Tagirov, Phys. Rev. Lett. **83**, 2058 (1999).
[6] A. I. Buzdin, A. V. Vedyayev, and N. V. Ryzhanova, Europhys. Lett. **48**, 686 (1999).
[7] V. Peña, Z. Sefrioui, D. Arias, C. Leon, J. Santamaria, J. L. Martinez, S. G. E. te Velthuis, and A. Hoffmann, Phys. Rev. Lett. **94**, 057002 (2005).
[8] N. M. Nemes *et al.*, Phys. Rev. B **78**, 094515 (2008).
[9] M. van Zalk, M. Veldhorst, A. Brinkman, J. Aarts, and H. Hilgenkamp, Phys. Rev. B **79**, 134509 (2009).
[10] T. Yamashita, H. Imamura, S. Takahashi, and S. Maekawa, Phys. Rev. B **67**, 094515 (2003).
[11] F. Giazotto, F. Taddei, F. Beltram, and R. Fazio, Phys. Rev. Lett. **97**, 087001 (2006).
[12] T. Holden *et al.*, Phys. Rev. B **69**, 064505 (2004).
[13] A. Hoffmann, S. G. E. te Velthuis, Z. Sefrioui, J. Santamaría, M. R. Fitzsimmons, S. Park, and M. Varela, Phys. Rev. B **72**, 140407(R) (2005).
[14] J. Chakhalian, J. W. Freeland, H. U. Habermeier, G. Cristiani, G. Khaliullin, M. van Veenendaal, and B. Keimer, Science **318**, 1114 (2007).
[15] Z. Sefrioui M. Varela, V. P. na, D. Arias, C. León, J. Santamaría, J. E. Villegas, J. L. Martínez, W. Saldarriaga, and P. Prieto, Appl. Phys. Lett. **81**, 4568 (2002).
[16] B. S. H. Pang, R. I. Tomov, and M. G. Blamire, Supercond. Sci. Technol. **17**, 624 (2004).
[17] A. Sawa, S. Kashiwaya, H. Obara, H. Yamasaki, M. Koyanagi, N. Yoshida, and Y. Tanaka, Physica C **339**, 287 (2000).
[18] Z. Y. Chen, A. Biswas, I. Žutić, T. Wu, S. B. Ogale, R. L. Greene, and T. Venkatesan, Phys. Rev. B **63**, 212508 (2001).
[19] P. Mikheenko, R. Chakalova, and C. M. Muirhead, Phys. Rev. B **71**, 184517 (2005).
[20] M. Huang, Z. Ivanov, P. Komissinski, and T. Claeson, Physica C **326-327**, 79 (1999).
[21] U. Schoop, M. Schonecke, S. Thienhaus, F. Herbstritt, J. Klein, L. Alff, and R. Gross, Physica C **350**, 237 (2001).
[22] H.-J. H. Smilde, H. Hilgenkamp, G. Rijnders, H. Rogalla, and D. H. A. Blank, Appl. Phys. Lett. **80**, 4579 (2002).
[23] G. Koster, B. L. Kropman, G. J. H. M. Rijnders, D. H. A. Blank, and H. Rogalla, Appl. Phys. Lett. **73**, 2920 (1998).
[24] J. R. Kirtley, M. B. Ketchen, K. G. Stawiasz, J. Z. Sun, W. J. Gallagher, S. H. Blanton, and S. J. Wind, Appl. Phys. Lett. **66**, 1138 (1995).
[25] S. Kashiwaya, Y. Tanaka, N. Yoshida, and M. R. Beasley, Phys. Rev. B **60**, 3572 (1999).
[26] J. A. Appelbaum, Phys. Rev. **154**, 633 (1967).
[27] Z. Sefrioui, D. Arias, V. Peña, J. E. Villegas, M. Varela, P. Prieto, C. León, J. L. Martinez, and J. Santamaria, Phys. Rev. B **67**, 214511 (2003).
[28] C. W. Jones, P. D. Battle, P. Lightfoot, and W. T. A. Harrison, Acta Crystallogr., Sect. C: Cryst. Struct. Commun. **45**, 365 (1989).
[29] R. Dömel, C. Horstmann, M. Siegel, A. I. Braginski, and M. Y. Kupriyanov, Appl. Phys. Lett. **67**, 1775 (1995).
[30] L. Antognazza, K. Char, T. H. Geballe, L. L. H. King, and A. W. Sleight, Appl. Phys. Lett. **63**, 1005 (1993).

[31] M. Gustafsson, E. Olsson, M. Q. Huang, P. V. Komissinski, P. B. Mozhaev, and Z. G. Ivanov, J. Low Temp. Phys. **117**, 575 (1999).
[32] Y. Yang, J. Gao, J. L. Sun, T. C. Chui, and L. Li, Physica C **300**, 151 (1998).
[33] J. G. Wen, N. Koshizuka, C. Traeholt, H. W. Zandbergen, E. M. C. M. Reuvekamp, and H. Rogalla, Physica C **255**, 293 (1995).
[34] R. C. Weast, *Handbook of Chemistry and Physics*, 53rd ed. (CRC Press, Boca Raton, FL, 1972).
[35] W. Si and X. X. Xi, Appl. Phys. Lett. **78**, 240 (2001).
[36] K. Semba, M. Mukaida, and A. Matsuda, Physica B **312-313**, 74 (2002).
[37] R. F. Egerton, *Electron Energy-Loss Spectroscopy in the Electron Microscope*, 2nd ed. (Plenum Press, New York, 1996).
[38] J. Mannhart and H. Hilgenkamp, Physica C **317-318**, 383 (1999).
[39] H. Hilgenkamp and J. Mannhart, Rev. Mod. Phys. **74**, 485 (2002).
[40] B. Chesca, D. Doenitz, T. Dahm, R. P. Huebener, D. Koelle, R. Kleiner, Ariando, H.-J. H. Smilde, and H. Hilgenkamp, Phys. Rev. B **73**, 014529 (2006).
[41] S. Yunoki, A. Moreo, E. Dagotto, S. Okamoto, S. S. Kancharla, and A. Fujimori, Phys. Rev. B **76**, 064532 (2007).
[42] J. R. Kirtley and D. J. Scalapino, Phys. Rev. Lett. **65**, 798 (1990).
[43] S. M. Sze and K. K. Ng, *Physics of Semiconductor Devices*, 3rd ed. (Wiley-Interscience, New York, 2007).
[44] C. Y. Chen, R. J. Birgeneau, M. A. Kastner, N. W. Preyer, and T. Thio, Phys. Rev. B **43**, 392 (1991).
[45] Y. Xu and J. W. Ekin, Phys. Rev. B **69**, 104515 (2004).
[46] M. P. de Jong, V. A. Dediu, C. Taliani, and W. R. Salaneck, J. Appl. Phys. **94**, 7292 (2003).
[47] D. W. Reagor, S. Y. Lee, Y. Li, and Q. X. Jia, J. Appl. Phys. **95**, 7971 (2004).
[48] M. Minohara, I. Ohkubo, H. Kumigashira, and M. Oshima, Appl. Phys. Lett. **90**, 132123 (2007).
[49] H. B. Michaelson, IBM J. Res. Dev. **22**, 72 (1978).
[50] K. Fröhlich *et al.*, Mater. Sci. Semicond. Process. **7**, 265 (2004).
[51] A. J. Hartmann, M. Neilson, R. N. Lamb, K. Watanabe, and J. F. Scott, Appl. Phys. A: Mater. Sci. Process. **70**, 239 (2000).
[52] X. Fang and T. Kobayashi, Appl. Phys. A: Mater. Sci. Process. **69**, S587 (1999).
[53] J. DeVries, S. S. Wakisaka, and R. E. Spjut, J. Mater. Res. **8**, 1497 (1993).
[54] G. Rietveld, N. Y. Chen, and D. van der Marel, Phys. Rev. Lett. **69**, 2578 (1992).
[55] S. Urazhdin, W. K. Neils, S. H. Tessmer, N. O. Birge, and D. J. Van Harlingen, Supercond. Sci. Technol. **17**, 88 (2004).
[56] T. Hirano, M. Ueda, K. Matsui, T. Fujii, K. Sakuta, and T. Kobayashi, Jpn. J. Appl. Phys., Part 2 **31**, L1345 (1992).
[57] S. I. Shkuratov, S. N. Ivanov, and S. N. Shilimanov, Surf. Sci. **266**, 224 (1992).
[58] D. Gu, S. K. Dey, and P. Majhi, Appl. Phys. Lett. **89**, 082907 (2006).
[59] R. J. Birgeneau *et al.*, Phys. Rev. B **38**, 6614 (1988).
[60] E. Dagotto, Rev. Mod. Phys. **66**, 763 (1994).
[61] M. Sato, S. Shamoto, J. M. Tranquada, G. Shirane, and B. Keimer, Phys. Rev. Lett. **61**, 1317 (1988).
[62] J. M. Tranquada, W. J. L. Buyers, H. Chou, T. E. Mason, M. Sato, S. Shamoto, and G. Shirane, Phys. Rev. Lett. **64**, 800 (1990).
[63] J. Rossat-Mignod, L. P. Regnault, M. J. Jurgens, C. Vettier, P. Burlet, J. Y. Henry, and G. Lapertot, Physica B **163**, 4 (1990).
[64] H. Y. Hwang, S.-W. Cheong, N. P. Ong, and B. Batlogg, Phys. Rev. Lett. **77**, 2041 (1996).